Gate-induced switching and negative differential resistance in a single-molecule transistor: Emergence of fixed and shifting states with molecular length

A. A. Farajian
Department of Mechanical Engineering and Materials Science, Rice University, Houston, Texas 77005

R. V. Belosludov, H. Mizuseki, and Y. Kawazoe
Institute for Materials Research, Tohoku University, Sendai 980-8577, Japan

T. Hashizume
Advanced Research Laboratory, Hitachi Ltd., Hatoyama, Saitama 350-0395, Japan

B. I. Yakobson
Department of Mechanical Engineering and Materials Science, Rice University, Houston, Texas 77005

The quantum transport of a gated polythiophene nanodevice is analyzed using density functional theory and nonequilibrium Green's function approach. For this typical molecular field effect transistor, we prove the existence of two main features of electronic components, i.e., negative differential resistance and good switching. *Ab initio* based explanations of these features are provided by distinguishing fixed and shifting conducting states, which are shown to arise from the interface and functional molecule, respectively. The results show that proper functional molecules can be used in conjunction with metallic electrodes to achieve basic electronics functionality at molecular length scales. © *2007 American Institute of Physics*. [DOI: 10.1063/1.2748047]

I. INTRODUCTION

The general field of molecular electronics[1–4] is currently being investigated very intensively in several scientific disciplines. Switching and negative differential resistance (NDR) are among the main features used in electronic and logic circuits nowadays, and are expected to play essential roles in molecular electronics as well. Theoretical and experimental investigations of these features at nanolength and molecular length scales have progressed substantially, providing better insight into characterization and design of miniaturized electronic and logic circuit elements.

Calculating transport in molecular wires including gate effect has been achieved by semiclassical derivation of transmission coefficient,[5] solving Schrödinger equation for the scattered electrons,[6] employing nonequilibrium Green's function (NEGF) formalism,[7–10] or solving Lippmann-Schwinger equation.[11] However, the existence and underlying mechanisms of NDR and swiching in gated molecular-scale devices are not fully understood, and further investigations are necessary. Using metallic electrodes such as gold in molecular field effect transistors (FETs), e.g., is shown to be problematic as the metal-induced gap states prevent abrupt switching,[7] even with ideal gate modulation. Here we show that a typical molecular FET shows both NDR and abrupt switching, which are explained based on *ab initio* analysis of the conducting states. We also show that the negative effects of the metal-induced states can be avoided if the functional molecule is longer than their generic decay length. Established nanolithography techniques can therefore be used to pattern metallic electrodes as interconnects between functional molecules. These results provide further insight into some of the basic issues of interest in molecular electronics.

II. MODEL AND METHODS

A. Optimized geometry

We consider a single-molecule FET, schematically depicted in Fig. 1(a), whose functional part is polythiophene. Polythiophene[12] is a conjugated polymer which has been studied extensively for possible applications, including molecular wires[13,14] and FETs.[15] We consider seven thiophene units (Fig. 1(b)) as they make the molecule long enough to assess the localization patterns of conducting states, while the calculations are computationally affordable. The functional molecule is assumed rigid and its vibrations are ignored. The molecule is attached to two semi-infinite gold electrodes by two sulfur atoms that act as clips. The positions of 22 gold atoms representing each electrode are extracted from bulk gold crystal with (111) surface, as depicted in Figs. 1(c) and 1(d).

The optimal orientations of the sulfur ends of polythiophene relative to the gold electrodes are obtained by minimizing the energy of a sulfur atom attached to one thiophene unit on Au(111) surface. Two series of structure relaxations are performed employing GAUSSIAN 98 program[16] with the method/basis B3PW91/LANL2MB, and two clusters of three and six gold atoms. These clusters are taken from one and two layers parallel to the surface, respectively, as is seen in Figs. 1(c) and 1(d), and both result in the same attachment geometry. We find that the sulfur ends of polythiophene are optimally located at hollow sites, i.e., above
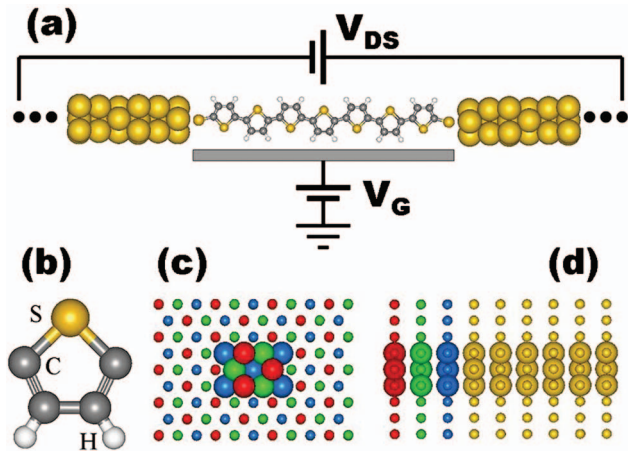
FIG. 1. (Color) (a) A polythiophene molecule, made up of individual thiophene units (b), attached to drain and source gold contacts via sulfur clips. Ideal gate modulation shifts the energy levels of the molecule. Front (c) and side (d) views of bulk gold crystal with (111) surface. The surface layer and the first and second underlying ones are distinguished by different colors. The electrodes of the nanodevice represented in (a) are extracted from bulk gold crystal with (111) surface, as highlighted by larger atomic sizes in (c) and (d).
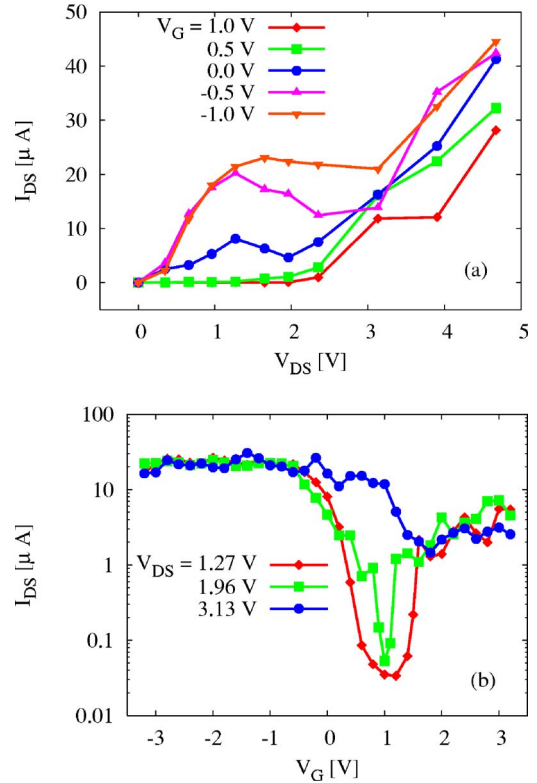

FIG. 2. (Color online) Drain-source current vs drain-source bias for different gate voltages (a), and drain-source current vs gate voltage for different drain-source biases (b).

the center of a surface gold triangle shown in Fig. 1(c), in accordance with other studies.[7,17] The distance between a sulfur clip and the center of the underlying gold triangle is determined to be 2.5 Å. After finding the geometry of attachment to the electrodes, a relaxed polythiophene molecule is introduced between the electrodes. The polythiophene with sulfur atoms at its ends is separately relaxed using the same method/basis. Therefore the junction geometry depicted in Fig. 1(a) is indeed the minimum energy configuration.

B. Quantum transport

For calculating transport properties, we employ the NEGF approach, implemented in our program TARABORD.[18] Using the contact atomic configurations of Fig. 1(a), the NEGF approach extends the contacts to infinity, causing each of them to resemble a semi-infinite nanowire. The NEGF method requires the specification of electronic structure of the system,[18] which is obtained by employing GAUSSIAN 98 program,[16] with the same method/basis used in geometry optimizations.

Upon applying drain-source bias, charge accumulates at the tip of each contact nanowire. In conducting atomic force microscope tips, similar effects have been modeled using point charges[19,21] with good agreement with the experimental results.[20,21] Here, we also model the charging effect by introducing a point charge between the first and the second tip layers of each electrode, and determine the drain-source potential drop by self-consistent calculation of the entire electronic structure. It should be mentioned that point charges less than $0.3e$ are enough to achieve the bias range reported here, with e being the absolute value of electron charge.

The Schrödinger equation in the nonorthogonal basis defined by the atomic orbitals of the molecule is $H_M\psi = \varepsilon S_M\psi$, where H_M is the Hamiltonian of the functional molecule, S_M is the basis overlap matrix, and ψ and ε are molecular eigen-

state and eigenvalue, respectively. We consider ideal gate modulation and assume that the molecular energy levels are shifted in response to gate bias according to

$$H_M \rightarrow H_M - eV_G S_M, \qquad (1)$$

where V_G is the gate bias. Equation (1) changes neither the electrode Hamiltonians nor the Hamiltonians coupling the electrodes to the molecule. This is in accordance with the fact that electrodes are considered parts of macroscopic reservoirs whose properties are independent of any change that might occur to the molecule sandwiched between them. The Hamiltonian and overlap matrices are used to calculate the transmission probability $T(E, V_{DS}, V_G)$ and conductance $G(E, V_{DS}, V_G) = (2e^2/h)T(E, V_{DS}, V_G)$,[18] where h is Planck's constant. The drain-source current I_{DS} is derived as

$$I_{DS} = \frac{2e}{h} \int_{-\infty}^{+\infty} dE T(E, V_{DS}, V_G)(f_D - f_S), \qquad (2)$$

where f_D and f_S are the Fermi-Dirac distributions of drain and source, with corresponding chemical potentials shifted by $\pm V_{DS}/2$ with respect to the zero-bias case (taken as reference potential).

III. RESULTS AND DISCUSSIONS

A. Current-voltage characteristics

The results of current calculations are shown in Fig. 2. The two most important features of the *I-V* curves in Fig. 2(a) are switching and NDR. Gate control is more pronounced at particular values of V_{DS}, such as $V_{DS} = 1.27$ V, to

the extent that the current is practically switched off by proper choice of the gate bias (the current decreases 714 times by changing V_G from −1.0 to 1.0 V at V_{DS}=1.27 V). The gate-induced switching observed here has some resemblance to the mechanical switching of current in bent carbon nanotube junction.[22]

The gate-induced switching can be observed more quantitatively in Fig. 2(b). Subthreshold slope S, a standard measure for comparison, is defined by the gate-voltage swing needed to reduce the current by one decade within the subthreshold region of *I-V* curve.[23] Therefore, smaller S means better switching. From Fig. 2(b), S is observed to be 100 mV/decade while increasing V_G from 1.5 to 1.6 V at V_{DS}=1.27 V, and 90 mV/decade while increasing V_G from 1.1 to 1.2 V at V_{DS}=1.96 V. These values of subthreshold slope S are larger than the ideal metal oxide semiconductor FET slope 60 mV/decade,[23] but superior to the slope 300 mV/decade calculated for a short (phenyl dithiol) molecule with ideal gate control.[7] The assumption of ideal gate modulation in Eq. (1) makes direct comparison with experimental results, such as nanotube FET slopes 70–80 mV/decade,[24] difficult. However, for relatively long functional molecules the insulating oxide layer can be realistically thick[7] and effective gate control is achievable, using, e.g., double[25] or all-around[26] gates. The specific electronic structure of polythiophene has its signature in the molecule local density of states (LDOS) within the NEGF approach. Device optimization, i.e., better subthreshold slopes and current on-off ratios, can be achieved by engineering the LDOS through proper choice of the functional molecule. Doping the molecule by individual dopant atoms is also effective, as it takes regions of LDOS with large variation of states under V_G into the integration window of Eq. (2), i.e., $f_D - f_S$.[27]

It should be mentioned that although we use specific drain-source bias values to explain the underlying mechanisms of switching and NDR, these features are observed for a range of drain-source biases, as is clearly seen from Fig. 2(a). Indeed Fig. 2(a) shows that gate-induced switching, i.e., significant change in current caused by changing gate bias while keeping drain-source bias V_{DS} fixed, is observed for the whole range $0.35 < V_{DS} < 2.35$. Similarly, for the NDR feature, depending on the gate bias V_G, Fig. 2(a) shows that NDR is observed for a range of V_{DS}, e.g., for V_G=0 V NDR is observed for the range $1.27 < V_{DS} < 1.96$, and for V_G=−0.5 V NDR is observed for the range $1.27 < V_{DS} < 2.35$. Particular drain-source biases such as 1.27 and 1.96 V are used in the text, and in Fig. 3, to clarify the underlying mechanism for typical values of the drain-source bias. Similar arguments can be used to explain switching and NDR for other drain-source biases within the ranges mentioned above.

B. Switching

The reason for current switching can be seen from the molecule LDOS and conductance characteristics depicted in Fig. 3. From Fig. 3(a) we observe that varying gate bias V_G results in shifting some of the conducting states within the integration window of Eq. (2). The peak at −0.18 eV for
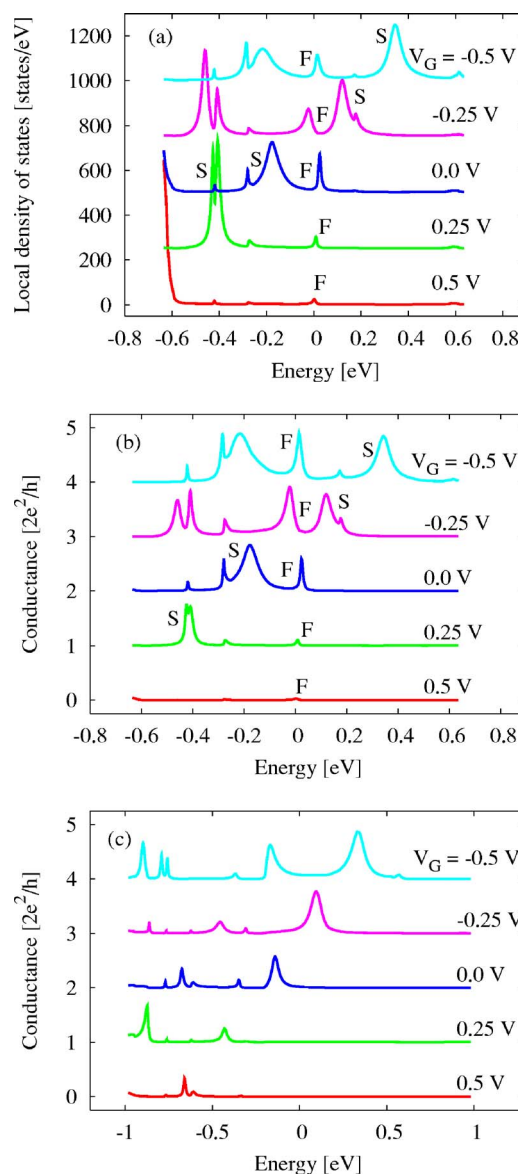

FIG. 3. (Color online) Local density of states at the molecule (a) and conductance characteristics (b) at different gate biases, with V_{DS} fixed at 1.27 V. Labels F and S indicate fixed and shifting states. (c) is similar to (b) but for V_{DS}=1.96 V. The curves for V_G=0.25, 0.0, −0.25, and −0.5 V are shifted vertically for clarity. The zero energy is the Fermi level of the system when it is under zero bias, as mentioned immediately after Eq. (2). In this figure, however, we show the properties of the system under bias. Therefore there is (electrochemical) potential drop along the molecule, which is self-consistently determined as explained in Sec. II B. The Fermi levels of the drain and source electrodes are pinned at ±1.27/2 V in (a) and (b), and at ±1.96/2 V in (c).

V_G=0.0 V corresponds to one of these shifting states. This peak shifts by the energy corresponding to the gate bias, $\Delta E = -eV_G$, as is seen for nonzero gate biases in Fig. 3(a), and expected from Eq. (1). The conductance curves of Fig. 3(b) clearly have the same general pattern as the LDOS curves of Fig. 3(a), indicating that the peaks of the LDOS curves represent conducting states through which carriers tunnel across the molecule. In addition to shifting states, however, there are some peaks in the curves of molecular LDOS of Fig. 3(a) and conductance of Fig. 3(b) whose energies do not change upon varying V_G (apart from occasional relatively small dislocations caused by nearby shifting

states). An example of these fixed peaks is the one at 0.03 eV for $V_G=0.0$ V. From Fig. 3(b) it is clear that the shifting and fixed states determine the behavior of conductance curves at different gate biases, which result in the *I-V* characteristics of Figs. 2(a) and 2(b). At a drain-source bias of 1.27 V, e.g., Fig. 3(b) shows that decreasing the gate bias V_G from 0.0 to −0.5 V brings some extra conducting states into the integration window of Eq. (2). At the same time, the conductance peak at the fixed-state energy 0.03 eV increases upon decreasing V_G. These effects result in an increase of current while changing V_G from 0.0 to −0.5 V, as is seen in Figs. 2(a) and 2(b). The reverse effect, i.e., substantial reduction of current, happens upon increasing V_G from 0.0 to 0.5 V, as it pushes the shifting conducting states out of the integration window of Eq. (2) and diminishes the conductance peaks corresponding to the fixed states.

C. Negative differential resistance

The NDR feature that is observed in Fig. 2(a), for example at $V_G=0$ can be explained by comparing the conductance curves at $V_{DS}=1.27$ and 1.96 V, depicted in Figs. 3(b) and 3(c), respectively. Increasing V_{DS} from 1.27 to 1.96 V in Fig. 2(a) results in a decrease in current. The conductance curves for $V_G=0.0$ V in Figs. 3(b) and 3(c) indicate that changing V_{DS} from 1.27 to 1.96 V causes a new set of conductance peaks, with larger interstate gaps and smaller areas under the peaks, to enter the integration window in Eq. (2). The current calculated for $V_{DS}=1.96$ V is therefore smaller than the current for $V_{DS}=1.27$ V. A similar argument explains current decrease for $V_G=-0.5$ V while increasing V_{DS} from 1.27 to 1.96 V. Different energy intervals in Figs. 3(b) and 3(c) result from different integration window widths for different drain-source biases.

It should be noticed that the contact-molecule couplings, used in calculating conductance,[18] change upon altering the potential drop across the molecule. The reason is that by changing V_{DS}, different energy states of the contacts (both localized at the surface and extended within) face the energy levels of the molecule. The energy levels of the molecule are also affected by the applied bias (we calculate the entire electronic structure under bias self-consistently, as explained in Sec. II B). All these effects cause the LDOS at the molecule and the conductance characteristics to depend on the applied bias. Accurate inclusion of the electronic structures of the contacts and the molecule is therefore essential in reliable transport calculations.

D. Fixed and shifting conducting states

It is natural to expect the energies of the molecule conducting states to shift upon varying V_G, in accordance with Eq. (1), not only for a finite cluster but also within the NEGF approach that attaches two semi-infinite electrodes to the molecule. The behavior of fixed states under applied gate bias, however, is not trivial. This behavior can be clarified by considering the length effect, i.e., the distribution of shifting and fixed conducting states along the molecule. Figure 4, shows decomposition of two typical shifting and fixed states, introduced in Figs. 3(a) and 3(b), along the molecule. These
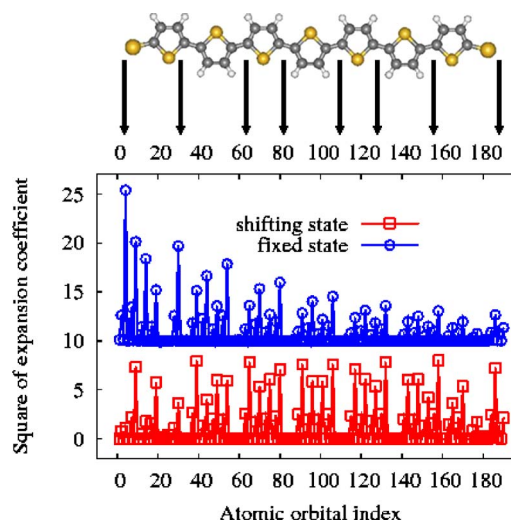

FIG. 4. (Color online) Squares of the coefficients for the shifting and fixed sample states introduced in Figs. 3(a) and 3(b) at $V_G=0$, in the expansion using atomic orbitals of the molecule as basis. The diagram of the fixed state is shifted vertically for clarity. The atomic orbital index spans the length of the molecule, as is seen from the correspondence shown at the top.

states correspond to the peaks at −0.18 (shifting) and 0.03 eV (fixed) for $V_G=0.0$ V. In Fig. 4, the horizontal axis indicates the atomic orbital index. Within the LANL2MB basis set used here, there are a total of 190 atomic orbitals (AOs) in the molecule region. These include one $3s$ and three $3p$ AOs for each sulfur atom, one $1s$ and four $2sp^3$-hybridized AOs for each carbon atom, and one $1s$ AO for each hydrogen atom. Orbital number 1 on the horizontal axis in Fig. 4 indicates the first ($3s$) AO of the sulfur atom attached to the left gold electrode, and orbital number 190 indicates the last ($3p$) AO of the sulfur atom attached to the right gold electrode. Therefore, the increase of atomic orbital index in Fig. 4 from 1 to 190 spans the length of the molecule from left to right. It is clear that the shifting state is distributed along the molecule without strong coupling to the electrodes, while the fixed state decays as one moves away from the molecule-electrode interface. In other words, shifting states have molecular orbital character, while fixed states are of the interface type. This observation is consistent with the application of gate bias V_G through Eq. (1), as the molecular orbitals are expected to shift and the interface states to be fixed, corresponding to the electrodes' characteristics not being affected by V_G. It should be noticed that the length effect, i.e., the length of the molecule being larger than generic decay length of the interface states, and the shifting molecular states not being coupled to the electrodes, is the key to understanding the improved switching behavior compared to short molecules.[7]

IV. CONCLUSIONS

In conclusion, the existence of two main features of electronic components are proved for a molecular-based field effect transistor. These features, i.e., negative differential resistance and abrupt switching, are explained by the localization of conducting states along the functional molecule and their redistribution under gate bias. The improved switching

character of this device compared to those based on shorter molecules is explained in terms of molecular length effects, which can eliminate the negative influence of the metallic electrodes, and pave the way for their application in molecular electronics.

[1] A. Aviram and M. A. Ratner, Chem. Phys. Lett. **29**, 277 (1974).
[2] J. R. Heath and M. A. Ratner, Phys. Today **56**(5), 43 (2003).
[3] N. Hush, Nat. Mater. **2**, 134 (2003).
[4] J. M. Seminario, Nat. Mater. **4**, 111 (2005).
[5] Y. Q. Feng, R. Q. Zhang, and S. T. Lee, J. Appl. Phys. **95**, 5729 (2004).
[6] E. Emberly and G. Kirczenow, Phys. Rev. B **62**, 10451 (2000).
[7] P. Damle, T. Rakshit, M. Paulsson, and S. Datta, IEEE Trans. Nanotechnol. **1**, 145 (2002).
[8] J. Taylor, H. Guo, and J. Wang, Phys. Rev. B **63**, 121104(R) (2001).
[9] F. Léonard and J. Tersoff, Phys. Rev. Lett. **88**, 258302 (2002).
[10] K. M. Indlekofer and J. Knoch, Phys. Rev. B **72**, 125308 (2005).
[11] M. Di Ventra and N. D. Lang, Phys. Rev. B **65**, 045402 (2001).
[12] M. Kobayashi, J. Chen, T. C. Chung, F. Moraes, A. J. Heeger, and F. Wuld, Synth. Met. **9**, 77 (1984).
[13] G. M. Tsivgoulis and J. M. Lehn, Adv. Mater. (Weinheim, Ger.) **9**, 39 (1997).
[14] R. V. Belosludov, A. A. Farajian, H. Mizuseki, K. Ichinoseki, and Y. Kawazoe, Jpn. J. Appl. Phys., Part 1 **43**, 2061 (2004).
[15] J. A. Merlo and C. D. Frisbie, J. Phys. Chem. B **108**, 19169 (2004).
[16] M. J. Frisch, G. W. Trucks, H. B. Schlegel *et al.*, GAUSSIAN 98, Revision A.11.1 2001, Gaussian, Inc., Pittsburgh PA.
[17] N. B. Larsen, H. Biebuyck, E. Delamarche, and B. Michel, J. Am. Chem. Soc. **119**, 3017 (1997).
[18] A. A. Farajian, R. V. Belosludov, H. Mizuseki, and Y. Kawazoe, Thin Solid Films **499**, 269 (2006).
[19] S. F. Lyuksyutov, P. B. Paramonov, R. A. Sharipov, and G. Sigalov, Phys. Rev. B **70**, 174110 (2004).
[20] S. F. Lyuksyutov, R. A. Vaia, P. B. Paramonov, S. Juhl, L. Waterhouse, R. M. Ralich, G. Sigalov, and E. Sancaktar, Nat. Mater. **2**, 468 (2003).
[21] G. Leatherman, E. N. Durantini, D. Gust, T. A. Moore, A. L. Moore, S. Stone, Z. Zhou, P. Rez, Y. Z. Liu, and S. M. Lindsay, J. Phys. Chem. B **103**, 4006 (1999).
[22] A. A. Farajian, B. I. Yakobson, H. Mizuseki, and Y. Kawazoe, Phys. Rev. B **67**, 205423 (2003).
[23] S. M. Sze, *Physics of Semiconductor Devices*, 2nd ed. (Wiley, New York, 1981).
[24] A. Javey, R. Tu, D. B. Farmer, J. Guo, R. G. Gordon, and H. Dai, Nano Lett. **5**, 345 (2005).
[25] E. Rauly, O. Potavin, F. Balestra, and C. Raynaud, Solid-State Electron. **43**, 2033 (1999).
[26] N. Singh, A. Agarwal, L. K. Bera, T. Y. Liow, R. Yang, S. C. Rustagi, C. H. Tung, R. Kumar, G. Q. Lo, N. Balasubramanian, and D.-L. Kwong, IEEE Electron Device Lett. **27**, 383 (2006).
[27] A. A. Farajian, K. Esfarjani, and Y. Kawazoe, Phys. Rev. Lett. **82**, 5084 (1999).